Title: Integrated pharmacodynamic analysis identifies two metabolic adaption pathways to metformin in breast cancer

Authors:

Simon. R. Lord[1,2,3*], Wei-Chen. Cheng[1], Dan. Liu[1], Edoardo. Gaude[4], Syed. Haider[5], Tom. Metcalf[6], Neel. Patel[7], Eugene. J. Teoh[1,2,7], Fergus. Gleeson[1,3,7], Kevin. Bradley[7], Simon. Wigfield[2], Christos. Zois[2], Daniel. R. McGowan[1], Mei-Lin. Ah-See[8], Alastair. M. Thompson[9], Anand. Sharma[1,2], Luc. Bidaut[10], Michael. Pollak[11], Pankaj. G. Roy[12], Fredrik. Karpe[13], Tim. James[14], Ruth. English[15], Rosie. F. Adams[15], Leticia Campo[3], Lisa. Ayers[16], Cameron Snell[17], Ioannis Roxanis[18], Christian. Frezza[4]†, John. D. Fenwick[6]†, Francesca. M. Buffa[1]†, Adrian. L. Harris[1,2,3]†

Affiliations:

[1]Department of Oncology, University of Oxford, Churchill Hospital, Oxford, OX3 7LE, UK

[2]Molecular Oncology Laboratories, Weatherall Institute of Molecular Medicine, University of Oxford, John Radcliffe Hospital, Oxford, OX3 9DS, UK

[3]NIHR Oxford Biomedical Research Centre, Oxford University Hospitals NHS Foundation Trust, Churchill Hospital, Oxford, OX3 7LE, UK

[4]MRC Cancer Unit, University of Cambridge, Hutchison/MRC Research Centre, Cambridge Biomedical Campus, Cambridge, CB2 0XZ, UK

[5]Breast Cancer Now Research Centre, The Institute of Cancer Research, London, SW3 6JB, UK

[6]Institute of Translational Medicine, University of Liverpool, Royal Liverpool University Hospital, Liverpool, L69 3GA, UK

[7]Department of Nuclear Medicine, Oxford University Hospitals NHS Foundation Trust, Churchill Hospital, Oxford, OX3 7LE, UK

[8]Department of Oncology, Luton and Dunstable Hospital, Luton, UK

[9]Department of Breast Surgical Oncology, MD Anderson Cancer Centre, Houston, 77030, USA

[10]College of Science, University of Lincoln, LN6 7TS, UK; formerly, Clinical Research Imaging Facility, University of Dundee, Ninewells Hospital, Dundee, DD2 1SY, UK

[11]Department of Oncology, McGill University, Montreal, H3T 1E2, Canada

[12]Breast Surgery Unit, Oxford University Hospitals NHS Foundation Trust, Churchill Hospital, Oxford, OX3 7LE, UK

[13]Oxford Centre for Diabetes, Endocrinology and Metabolism, Radcliffe Department of Medicine, University of Oxford, Churchill Hospital, Oxford, OX3 7LE, UK

[14]Department of Clinical Biochemistry, Oxford University Hospitals NHS Foundation Trust, John Radcliffe Hospital, Oxford, OX3 9DU, UK

[15]Oxford Breast Imaging Centre, Oxford University Hospitals NHS Foundation Trust, Oxford, OX3 7LE, UK

[16]Department of Clinical and Laboratory Immunology, Oxford University Hospitals NHS Foundation Trust, Churchill Hospital, Oxford, OX3 7LE, UK

[17]Department of Anatomical Pathology, Mater Research Institute, Brisbane, 4101, Australia

[18]Department of Cellular Pathology, Oxford University Hospitals NHS Foundation Trust, John Radcliffe Hospital, Oxford, OX3 9DU, UK

* Lead contact and correspondence: simon.lord@oncology.ox.ac.uk

† Senior authors contributed equally to the work

SUMMARY:

Late phase clinical trials investigating metformin as a cancer therapy are underway. However, there remains controversy as to the mode of action of metformin in tumours at clinical doses. We conducted a clinical study integrating measurement of markers of systemic metabolism, dynamic FDG-PET-CT, transcriptomics and metabolomics at paired time points to profile the bioactivity of metformin in primary breast cancer. We show metformin reduces the levels of mitochondrial metabolites, activates multiple mitochondrial metabolic pathways and increases 18-FDG flux in tumours. Two tumour groups are identified with distinct metabolic responses, an OXPHOS transcriptional response group for which there is an increase in OXPHOS gene transcription and an FDG response group with increased 18-FDG uptake. Increase in proliferation, as measured by a validated proliferation signature, suggested patients in the OTR group were resistant to metformin treatment. We conclude that mitochondrial response to metformin in primary breast cancer may define anti-tumour effect.

Keywords:

Metformin, Breast cancer, Dynamic PET-CT, Transcriptomics, Metabolomics

INTRODUCTION:

Metformin can reduce proliferation of cancer cell lines in vitro and in vivo and this effect has been ascribed to inhibition of mitochondrial complex 1 (Wheaton et al., 2014). However, the doses of metformin used have typically been 10-1000 fold greater than peak plasma level in humans (Dowling et al., 2012). Hence controversy remains as to whether metformin's effects on tumour metabolism at clinical doses are determined by its direct effects on mitochondria or through its action on systemic metabolism via AMPK dependent inhibition of hepatic gluconeogenesis and subsequent reduced circulating glucose and insulin levels.

Several window trials have used immunohistochemistry to investigate metformin's clinical effects in breast, endometrial and prostate cancer. A number have shown that metformin can reduce the proliferation marker Ki67 but no singular mechanism has been clearly demonstrated. Activation of AMPK suggestive of an energy stress has been observed whilst other studies have demonstrated reduced pAKT consistent with decreased insulin signaling (Dowling et al., 2015; Hadad et al., 2011; Schuler et al., 2015). Recently published work by Liu et al comparing the metabolite profile of 10 ovarian tumour samples from patients on metformin versus 10 control samples (patients not on metformin) demonstrated decreases in the levels of some TCA cycle intermediates and short-chain acyl-carnitines. Additionally, the response to metformin seen in the human metabolite profiles could be recapitulated in a mouse model and in vitro when nutrient concentrations were limited (Liu et al., 2016). To date this is the most convincing clinical evidence that metformin has significant and measurable mitochondrial effects at standard therapeutic doses. Here, we present the results of a clinical study that integrates tumour metabolomic profiling with dynamic

imaging, transcriptomics, and systemic metabolic markers to further dissect the effects of metformin on systemic and breast tumour metabolism.

We recruited 40 female patients with treatment-naïve primary breast cancer to the study. Before and after a 13–21 day course of metformin patients underwent a dynamic fluoro-deoxy-D-glucose positron emission tomography-computed tomography (FDG-PET-CT) scan, breast core biopsies from the primary tumour under ultrasound guidance, and blood samples to assay host metabolic markers of the insulin axis (**Fig. 1a**). See **Table S1** for details of study entry criteria and **Table S2** for tumour features. See online methods for further detail.

RESULTS AND DISCUSSION:

Metformin increases FDG flux into primary breast tumours

Pre-clinical data has shown that inhibition of oxidative phosphorylation (OXPHOS) by metformin increases dependence on glycolysis (Ben Sahra et al., 2010; Birsoy et al., 2014; Wheaton et al., 2014). The FDG radio-tracer is a marker of tissue glucose utilization. Kinetics analysis of FDG uptake time-courses obtained from dynamic PET images potentially provides more consistent measures of tumour tracer uptake, adjusted for variations in tracer inflow to the tumour, than standard static FDG-PET-CT (Dunnwald et al., 2011). Using an irreversible 2-tissue compartment model describing rates of FDG transport and phosphorylation (see methods) we observed an increase in FDG flux (K_{FDG}) into the primary breast cancer following metformin (**Fig. 1b**) but no change in the static uptake measures SUL_{max} and SUL_{mean} for tumour (standardised uptake values normalised for lean body mass) (**Fig. S1a-b and Table S3**). There was no change in nodal SUL_{max} for patients with FDG avidity

within ipsilateral axillary lymph nodes (**Fig. S1c**). There was a significant correlation between change in K_{FDG} in the primary tumour and change in SUL_{max} in the axillary nodes (**Fig. S1d**).

The above findings infer that metformin treatment leads to increased glucose uptake by breast tumours and this would be consistent with a switch to glycolytic metabolism. Additionally, the analysis emphasises the sensitivity of dynamic FDG-PET over static scanning in identifying subtle pharmacodynamic changes in glucose metabolism. If normal tissues such as liver absorbed more FDG in response to metformin, FDG activity concentrations in the blood would fall, potentially reducing FDG uptake by the tumour. However, the compartment model / flux constant approach describes tumour FDG uptake after allowing for differences across the whole time-course of the dynamic scan in levels of blood-borne tracer flowing into the tumour, determined from imaged activity concentrations in the descending aorta. It is possible that it is precisely because this model controls for the flow of tracer into the tumour that we see a significant change in the flux constant and not SUV on static PET scanning.

Two tumour groups with distinct metabolic responses to metformin

We did not observe changes in the levels of the TCA cycle intermediates citrate, succinate, fumarate and malate in contrast to Liu et al (Liu et al., 2016), or asparate, a key marker of electron transport chain integrity (**Fig. 1c**). Ornithine is condensed with carbamoyl phosphate to produce citrulline in the only intra-mitochondrial reaction of the urea cycle and citrulline levels decreased (mean log2FC=-0.53; p=0.007). Some investigators have observed an increase in the ADP/ATP and AMP/ATP ratios typically under in vitro nutrient deprived conditions but there was no significant increase in intratumoural ADP/ATP or AMP/ATP ratios post-metformin (**Fig. S1e**) and this is consistent with metabolomic data

from ovarian tumours published in Liu et al (Liu et al., 2016). The discordance in findings with metabolomic profiling from preclinical studies may reflect the heterogeneity inherent in a study analysing clinical samples and difficulty of making very precise measurements when there may be only small changes in the levels of these metabolites. Mitochondrial dysfunction under the tissue culture conditions described in the literature cited above is likely to be greater than in our study. Indeed, Gaude et al showed that at lower levels of mitochondrial dysfunction there was little or no decrease in TCA cycle metabolites and aspartate (Gaude et al., 2018). Uptake from the stroma in an in vivo system may help maintain aspartate levels (for example Birsoy et al used a cell line lacking in the transporter SLC1A3 which was expressed at the mRNA level in our clinical samples) (Birsoy et al., 2015). In contrast to findings in some other studies (Dowling et al., 2015; Hadad et al., 2011) tumour immunohistochemistry demonstrated no change in AMPK phosphorylation following metformin (paired t-test, p=0.801) (**Fig. S1f**). There was no correlation between change in pAMPK and change in K_{FDG} (**Fig. S1g**).

Whole transcriptome RNA sequencing pre- and post-metformin revealed significant upregulation of several pathways linked to metabolism (**Fig. 2a**) and more specifically to mitochondrial pathways and disease (**Table S4**). This included four KEGG pathways that we predicted would be targeted by metformin based on extensive pre-clinical data (Birsoy et al., 2014; Fendt et al., 2013; Liu et al., 2016; Mullen et al., 2011; Wheaton et al., 2014): oxidative phosphorylation (KEGG:00190); TCA cycle (KEGG:00020); glycolysis and gluconeogenesis (KEGG:00010); alanine, aspartate and glutamate metabolism (KEGG:00250). Taking all genes that were significantly up or down regulated from these pathways we observed that for one hierarchical cluster of patients fold change in expression was strikingly increased for this set of genes (OXPHOS responders or OTR). All patients in the

OTR group were oestrogen receptor positive (**Fig. 2b**). Coherent with this observation, unsupervised hierarchical clustering of the expressed nuclear whole transcriptome showed that patients in the OTR group also clustered together in this analysis (**Fig. S2a**). Notably clustering of the OTR group also occurred for expressed genes of the mitochondrial transcriptome (**Fig. S2b**). For patients with limited OXPHOS transcriptional response there was evidence of increased glucose uptake defined by an increase in K_{FDG} (FDG responders or FR) in contrast to the OTR group.

Consistent with mitochondrial targeting it has recently been shown that metformin treatment leads to a decrease in the levels of short chain acyl-carnitines in ovarian cancer (Liu et al., 2016). Metabolomic profiling of paired pre- and post-metformin samples showed that acetyl- and propionylcarnitine levels decrease (mean $\log_2$FC=-1.32, p=0.046 and $\log_2$FC=-1.01, p=0.039, respectively). Acetylcarnitine is a short-chain acyl-carnitine derived from glucose carbons (Schooneman et al., 2013) and in contrast to the OTR group their FR counterparts were able to maintain acetylcarnitine levels (**Fig. 2c**). There was a strong correlation between change in K_{FDG} and change in acetylcarnitine levels (**Fig. 2d**). **Fig. S2c** shows the interquartile range and median fold change for metabolites in the OTR and FR groups. It is unclear why intratumoural acetylcarnitine levels dropped and this finding is at odds with Chen et al who showed that complex 1 inhibition in a cell line model resulted in a several fold increase in acetylcarnitine levels within whole cells and mitochondria (Chen et al., 2016). However, this may be due to the discordance between the very different environmental conditions and strength of mitochondrial inhibition in our clinical study compared to cell line models. Additionally, Chen et al only assayed the mitochondrial matrix, and used a different complex 1 inhibitor in a non-breast cancer model. Notably, carnitine o-acetyltransferase which catalyses the bidirectional conversion of acetylcarnitine

to acetyl-CoA within both mitochondria and peroxisomes was differentially upregulated in the OTR group (**all Fig. 3a**). Hence, we speculate that altered flux in this pathway may be a consequence of metformin treatment. The positive correlation between change in FDG flux and intratumoural acetylcarnitine levels possibly reflects increased flux of glucose carbons toward acetyl-CoA. To fully understand the effects of metformin and mitochondrial defects on acyl-carnitine metabolism will require further work in preclinical models.

Maintaining aspartate levels has been shown to be a key resistance mechanism to electron transport chain inhibition and biguanides (Birsoy et al., 2015; Cardaci et al., 2015; Sullivan et al., 2015). There was no difference in aspartate metabolite levels between the FR and OTR groups (**Fig. 1c and S3a**). However, several genes involved in aspartate metabolism were significantly upregulated and it was striking that the increase in expression of 3 of the 5 genes that encode for units of the malate-aspartate shuttle (GOT2, MDH1 and MDH2) was significantly greater in the OTR group compared to the FR group (**Fig. 3a**). Dependency on glutamine as a source of citrate for either lipid or aspartate biosynthesis has been shown to be a key resistance mechanism to metformin and other mitochondrial insults (Birsoy et al., 2015; Fendt et al., 2013; Mullen et al., 2011) and we observed increased expression of multiple genes that regulate glutamine metabolism. Two key checkpoints in this process were differentially upregulated in the OTR group, mitochondrial isocitrate dehydrogenase (IDH2) and the citrate transporter, SLC25A1, which delivers glutamine derived citrate to the cytosol where it is cleaved by ATP citrate lyase to oxaloacetate and acetyl-CoA for aspartate and lipid synthesis, respectively (**Fig. 3a**). Previous work has also shown that both isoforms of isocitrate dehydrogenase, IDH1 and IDH2, support growth in cells that use glutamine dependent reductive carboxylation. Hence, tumours harbouring IDH mutations may be more susceptible to biguanide therapy.

Systemic response to metformin does not correlate with change in intra-tumoural assays

Metformin has been shown to modulate a number of systemic metabolic and inflammatory markers in diabetic populations. In our study metformin lowered circulating levels of serum glucose, insulin, c-peptide, and an insulin resistance score (homeostatic model assessment or HOMA) but not leptin, adiponectin, C-reactive protein, tumour necrosis factor alpha or interleukin 6 (**Fig. 3b, S3b and Table S5**). However, there were no significant differences between the OTR and FR groups in pre/post metformin changes in levels of any of these circulating metabolic markers (**Fig. S3c**). There was a marked overlap in genes whose change in expression correlated with change in K_{FDG} and change in acetylcarnitine (hypergeometric test, $p<0.00001$), but little corresponding overlap with genes related to change in c-peptide, glucose, insulin or HOMA (**Fig. 3c and S3d**). Eighteen of the genes correlating with change in K_{FDG} and acetylcarnitine were KEGG annotated metabolism genes most notably associated with oxidative phosphorylation, carbohydrate, amino acid and nucleotide metabolism pathways (**Table S6**). There was an increase in pAKT expression on tumour immunohistochemistry (paired t-test, $p=0.026$) but no correlation between change in pAKT expression and change in c-peptide, glucose, insulin or HOMA and no significant difference between the FR and OTR groups (**Fig S3e-g**). There was also no difference in pAMPK expression between the FR and OTR groups (**Fig S3g**).

The increase in tumour pAKT expression was unexpected and not consistent with a decrease in insulin receptor signalling or findings in prior studies. AKT activation increases ATP levels in cells and has been identified in a number of studies as being a key player in the regulation of both glycolysis and oxidative phosphorylation (Robey and Hay, 2009). Recent work has shown mitochondrial AKT activation occurs in the context of tumour energy and hypoxic

stress switching metabolism toward glycolysis (Chae et al., 2016). However, we cannot exclude metformin's systemic effects on host metabolism being a significant factor in modulating tumour metabolism and proliferation and indeed we would expect a decrease in insulin levels to have some effect on tumour intracellular signalling. Our study only recruited patients with normal systemic glucose levels and for patients with diabetes or glucose intolerance any effect on insulin signalling via the hypoglycaemic activity of metformin is likely to be greater.

We then investigated the relationship between tumour metformin levels and metabolic response. Although serum and tumour levels were significantly correlated with each other (**Fig. 3d)** they did not differ between the OTR and FR groups **(Fig. S4a**). Previously published preclinical data suggested that expression of the organic cation transporter, OCT1, is required for tumour uptake of metformin and metabolic response (Chandel et al., 2016; Dowling et al., 2016). There was no significant correlation between baseline OCT1 gene expression and tumour metformin levels but notably the patient with highest tumour metformin levels also had the greatest expression of tumour OCT1 (**Fig. S4b)**. Furthermore, there was no difference in baseline OCT1 expression between the OTR and FR groups (**Fig. S4c)**. Baseline OCT1 expression did correlate with change in K_{FDG} although the relevance of this finding is unclear given that there was no such relationship with tumour metformin levels (**Fig. S4d)**.

Glucose transporter gene expression may determine sensitivity of cell lines to biguanides (Birsoy et al., 2014). Expression of the glucose transporter, GLUT1, has previously been shown to correlate with uptake of FDG on PET-CT (Bos et al., 2002) and in our study change in K_{FDG} positively correlated with the change in expression of GLUT1 (**Fig. 3e**). However,

there was no significant difference in GLUT1 expression between the 2 groups although there was for another glucose transporter, GLUT4 (**Fig. S4e**).

OXPHOS transcriptional response to metformin relates to change in a proliferation metagene

Several clinical studies have shown that metformin can reduce breast, prostate and endometrial cancer cell proliferation (Hadad et al., 2011; Joshua et al., 2014; Laskov et al., 2014; Mitsuhashi et al., 2014; Niraula et al., 2012; Schuler et al., 2015). We explored the effect of metformin on a validated human breast cancer proliferation signature (Desmedt et al., 2008) and overall observed no significant change following metformin treatment (**Fig. 4**). However, it was striking that an increase in metagene expression occurred in the OTR group but in contrast there was a decrease for several patients in the FR group, the change in metagene expression consequently differing significantly between the 2 groups (**Fig. 4**). Under in vitro low glucose conditions the ability for cell lines to upregulate OXPHOS predicts for sensitivity to biguanides (Birsoy et al., 2014) and our data suggests that a reactive increase in OXPHOS and aspartate synthesis gene transcription may be critical for resistance to metformin. None of the circulating or tumour immunohistochemical markers, metformin levels, K_{FDG}, or significantly altered metabolites correlated with change in expression of the proliferation metagene (**Fig S4f**).

Conclusion and perspectives:

Our work outlines two types of breast cancer metabolic response to metformin and links the effects of metformin on mitochondrial metabolism with its effects on breast cancer proliferation at a transcriptional level. Tumours that were able to upregulate OXPHOS gene

transcription in response to metformin showed an increase in their proliferation score suggestive of resistance following metformin treatment.

The upregulation of multiple transcriptomic pathways involved in mitochondrial metabolism and decrease in levels of several intratumoural mitochondrial metabolites is suggestive of metformin interfering with mitochondrial metabolism. Furthermore, the increased expression of multiple genes regulating glycolysis and glucose transport alongside our imaging data is consistent with mobilisation of glucose metabolism in response to metformin. The upregulation of key regulatory genes for glycolysis, aspartate and glutamine metabolism in response to metformin may represent a mechanism of resistance and confirms the potential of previously proposed strategies to target these pathways, for example by combining biguanides with glutaminase inhibitors or dichloroacetate (Fendt et al., 2013; Haugrud et al., 2014). Oestrogen receptor expression may also act as a biomarker to distinguish the 2 types of metabolic response. Amongst the most likely determinants for resistance in our view are mitochondrial defects (for example mutations in complex 1 genes) and this would be consistent with in vitro data (Birsoy et al., 2014). Hence, we propose that translational work within ongoing phase 3 trials should investigate whether mitochondrial mutations herald biguanide sensitivity and clinical outcome. However, we emphasise that early dynamic monitoring of response may detect the heterogeneity that cannot be detectable at baseline.

There have been a number of other window studies designed to assess metformin's pharmacodynamic effects in several different tumour types and it is important to note the differences to this study. Most of these trials have used immunohistochemical approaches on a wide range of markers but in particular Ki67, AMPK, and markers of apoptosis with discrepant results (Dowling et al., 2015; Hadad et al., 2011; Schuler et al., 2015). The most

in-depth clinical study to date to use metabolomic approaches, Liu et al, suggested some evidence of mitochondrial interference but in contrast to our study did not take serial biopsies to allow identification of differential types of response and was limited to effectively one assay. Additionally, Liu et al assayed samples taken from 10 patients with ovarian cancer that happened to be receiving metformin for diabetes whilst using control samples from non-diabetic patients with a lower mean body mass index. Hence, this was a comparison between two patient groups with distinct host metabolism (Liu et al., 2016). In contrast this study only recruited from a non-diabetic population, the focus of ongoing phase 3 trials.

These data are consistent with several of the observations seen previously using in vitro and in vivo models but it is still uncertain whether these perturbations are enough for metformin to deliver clinical benefit to patients. A recent substudy of the ALTTO phase 3 adjuvant breast cancer trial reported a strong association between metformin and improved overall survival in diabetic patients (Sonnenblick et al., 2017). Our observations make the case for the continued clinical study of metformin and more potent biguanides (Zhang et al., 2016) in non-diabetic patients. The results of ongoing phase 3 trials are awaited (Gillessen et al., 2016; Goodwin et al., 2015).

Limitations of study:

This study had no control arm and hence it is possible that some of the observations could be related to the passage of time or interventions (e.g. biopsies). Given the nature of this clinical translational study the analysis especially relies on correlative evaluation and hence we cannot rule out a link between the systemic effects of metformin and significant changes

in tumour metabolism and proliferation. Although 40 patients are a substantial number for an involved pharmacodynamic study of this type, correlations across the assays were not able to carried out across the full cohort for varied reasons (technical difficulties with some scans and insufficient sample to carry out all assays, etc) and increased recruitment would provide greater power for the analyses.

Acknowledgments:

Funding for this study was provided by the Oxford Cancer Imaging Centre (funded by Cancer Research UK and the Engineering and Physical Sciences Research Council), the Oxford Biomedical Research Centre and the Breast Cancer Research Foundation, whilst the work of CF and EG was funded by a core fund from the Medical Research Council. The circulating glucose, insulin, c-peptide and c-reactive protein assays were carried out by the Oxford Clinical Biochemistry Laboratory, circulating IL-6 and TNF-alpha assays by the Oxford Clinical Immunology Laboratory (both Oxford University Hospitals NHS Foundation Trust) and adiponectin and leptin by the Core Biochemical Assay Laboratory, Cambridge University Hospitals NHS Foundation Trust. The immunohistochemistry assays were carried out by the GCP laboratory, Department of Oncology, University of Oxford.

Author contributions:

SL and AH designed the study. SL, AT and AH co-supervised the clinical implementation of the study. SL, AH, AT, MA, AS, PR, RE, and RA recruited patients to the clinical trial, collected the clinical data and carried out the study procedures. DL, TM, NP, DM, KB, FG, LB and ET carried out the imaging analysis with overall supervision of the project from JF. EG performed the metabolomics analyses of the clinical samples with supervision form CF. SL,

TJ, LC, LA, CZ and SW carried out the tissue and serum-based assays. CS and IR scored the immunohistochemistry assays. WC and SH performed the bioinformatics and statistical analyses with supervision from FB and SL. AM, FK and MP provided advice on the design of the study and the analysis. SL wrote the manuscript with input from the other authors.

Declarations of interest:

The authors declare no competing interests.

References:

Anders, S., and Huber, W. (2010). Differential expression analysis for sequence count data. Genome Biol *11*, R106.

Ben Sahra, I., Laurent, K., Giuliano, S., Larbret, F., Ponzio, G., Gounon, P., Le Marchand-Brustel, Y., Giorgetti-Peraldi, S., Cormont, M., Bertolotto, C., et al. (2010). Targeting cancer cell metabolism: the combination of metformin and 2-deoxyglucose induces p53-dependent apoptosis in prostate cancer cells. Cancer Res *70*, 2465-2475.

Bertoldo, A., Peltoniemi, P., Oikonen, V., Knuuti, J., Nuutila, P., and Cobelli, C. (2001). Kinetic modeling of [(18)F]FDG in skeletal muscle by PET: a four-compartment five-rate-constant model. Am J Physiol Endocrinol Metab *281*, E524-536.

Birsoy, K., Possemato, R., Lorbeer, F.K., Bayraktar, E.C., Thiru, P., Yucel, B., Wang, T., Chen, W.W., Clish, C.B., and Sabatini, D.M. (2014). Metabolic determinants of cancer cell sensitivity to glucose limitation and biguanides. Nature *508*, 108-112.

Birsoy, K., Wang, T., Chen, W.W., Freinkman, E., Abu-Remaileh, M., and Sabatini, D.M. (2015). An Essential Role of the Mitochondrial Electron Transport Chain in Cell Proliferation Is to Enable Aspartate Synthesis. Cell *162*, 540-551.

Bos, R., van Der Hoeven, J.J., van Der Wall, E., van Der Groep, P., van Diest, P.J., Comans, E.F., Joshi, U., Semenza, G.L., Hoekstra, O.S., Lammertsma, A.A., et al. (2002). Biologic correlates of (18)fluorodeoxyglucose uptake in human breast cancer measured by positron emission tomography. J Clin Oncol *20*, 379-387.

Cardaci, S., Zheng, L., MacKay, G., van den Broek, N.J., MacKenzie, E.D., Nixon, C., Stevenson, D., Tumanov, S., Bulusu, V., Kamphorst, J.J., et al. (2015). Pyruvate carboxylation enables growth of SDH-deficient cells by supporting aspartate biosynthesis. Nat Cell Biol *17*, 1317-1326.

Chae, Y.C., Vaira, V., Caino, M.C., Tang, H.Y., Seo, J.H., Kossenkov, A.V., Ottobrini, L., Martelli, C., Lucignani, G., Bertolini, I., et al. (2016). Mitochondrial Akt Regulation of Hypoxic Tumor Reprogramming. Cancer Cell *30*, 257-272.

Chandel, N.S., Avizonis, D., Reczek, C.R., Weinberg, S.E., Menz, S., Neuhaus, R., Christian, S., Haegebarth, A., Algire, C., and Pollak, M. (2016). Are Metformin Doses Used in Murine Cancer Models Clinically Relevant? Cell Metab *23*, 569-570.

Chen, W.W., Freinkman, E., Wang, T., Birsoy, K., and Sabatini, D.M. (2016). Absolute Quantification of Matrix Metabolites Reveals the Dynamics of Mitochondrial Metabolism. Cell *166*, 1324-1337 e1311.

Desmedt, C., Haibe-Kains, B., Wirapati, P., Buyse, M., Larsimont, D., Bontempi, G., Delorenzi, M., Piccart, M., and Sotiriou, C. (2008). Biological processes associated with breast cancer clinical outcome depend on the molecular subtypes. Clin Cancer Res *14*, 5158-5165.

Dowling, R.J., Lam, S., Bassi, C., Mouaaz, S., Aman, A., Kiyota, T., Al-Awar, R., Goodwin, P.J., and Stambolic, V. (2016). Metformin Pharmacokinetics in Mouse Tumors: Implications for Human Therapy. Cell Metab *23*, 567-568.

Dowling, R.J., Niraula, S., Chang, M.C., Done, S.J., Ennis, M., McCready, D.R., Leong, W.L., Escallon, J.M., Reedijk, M., Goodwin, P.J., et al. (2015). Changes in insulin receptor signaling underlie neoadjuvant metformin administration in breast cancer: a prospective window of opportunity neoadjuvant study. Breast Cancer Res *17*, 32.

Dowling, R.J., Niraula, S., Stambolic, V., and Goodwin, P.J. (2012). Metformin in cancer: translational challenges. J Mol Endocrinol *48*, R31-43.

Dunnwald, L.K., Doot, R.K., Specht, J.M., Gralow, J.R., Ellis, G.K., Livingston, R.B., Linden, H.M., Gadi, V.K., Kurland, B.F., Schubert, E.K., et al. (2011). PET tumor metabolism in locally advanced breast cancer patients undergoing neoadjuvant chemotherapy: value of static versus kinetic measures of fluorodeoxyglucose uptake. Clin Cancer Res *17*, 2400-2409.

Fendt, S.M., Bell, E.L., Keibler, M.A., Davidson, S.M., Wirth, G.J., Fiske, B., Mayers, J.R., Schwab, M., Bellinger, G., Csibi, A., et al. (2013). Metformin decreases glucose oxidation and increases the dependency of prostate cancer cells on reductive glutamine metabolism. Cancer Res *73*, 4429-4438.

Gaude, E., Schmidt, C., Gammage, P.A., Dugourd, A., Blacker, T., Chew, S.P., Saez-Rodriguez, J., O'Neill, J.S., Szabadkai, G., Minczuk, M., et al. (2018). NADH Shuttling Couples Cytosolic Reductive Carboxylation of Glutamine with Glycolysis in Cells with Mitochondrial Dysfunction. Mol Cell *69*, 581-593 e587.

Gillessen, S., Gilson, C., James, N., Adler, A., Sydes, M.R., Clarke, N., and Group, S.T.M. (2016). Repurposing Metformin as Therapy for Prostate Cancer within the STAMPEDE Trial Platform. Eur Urol *70*, 906-908.

Goodwin, P.J., Parulekar, W.R., Gelmon, K.A., Shepherd, L.E., Ligibel, J.A., Hershman, D.L., Rastogi, P., Mayer, I.A., Hobday, T.J., Lemieux, J., et al. (2015). Effect of metformin vs placebo on and metabolic factors in NCIC CTG MA.32. J Natl Cancer Inst *107*.

Hadad, S., Iwamoto, T., Jordan, L., Purdie, C., Bray, S., Baker, L., Jellema, G., Deharo, S., Hardie, D.G., Pusztai, L., et al. (2011). Evidence for biological effects of metformin in operable breast cancer: a pre-operative, window-of-opportunity, randomized trial. Breast Cancer Res Treat *128*, 783-794.

Haugrud, A.B., Zhuang, Y., Coppock, J.D., and Miskimins, W.K. (2014). Dichloroacetate enhances apoptotic cell death via oxidative damage and attenuates lactate production in metformin-treated breast cancer cells. Breast Cancer Res Treat *147*, 539-550.

Hume, R. (1966). Prediction of lean body mass from height and weight. J Clin Pathol *19*, 389-391.

Joshua, A.M., Zannella, V.E., Downes, M.R., Bowes, B., Hersey, K., Koritzinsky, M., Schwab, M., Hofmann, U., Evans, A., van der Kwast, T., et al. (2014). A pilot 'window of opportunity' neoadjuvant study of metformin in localised prostate cancer. Prostate Cancer Prostatic Dis *17*, 252-258.

Laskov, I., Drudi, L., Beauchamp, M.C., Yasmeen, A., Ferenczy, A., Pollak, M., and Gotlieb, W.H. (2014). Anti-diabetic doses of metformin decrease proliferation markers in tumors of patients with endometrial cancer. Gynecol Oncol *134*, 607-614.

Liu, D., Chalkidou, A., Landau, D.B., Marsden, P.K., and Fenwick, J.D. (2014). 18F-FLT uptake kinetics in head and neck squamous cell carcinoma: a PET imaging study. Med Phys *41*, 041911.

Liu, X., Romero, I.L., Litchfield, L.M., Lengyel, E., and Locasale, J.W. (2016). Metformin Targets Central Carbon Metabolism and Reveals Mitochondrial Requirements in Human Cancers. Cell Metab *24*, 728-739.

McCarthy, D.J., Chen, Y., and Smyth, G.K. (2012). Differential expression analysis of multifactor RNA-Seq experiments with respect to biological variation. Nucleic Acids Res *40*, 4288-4297.

Mehta, S., Hughes, N.P., Li, S., Jubb, A., Adams, R., Lord, S., Koumakis, L., van Stiphout, R., Padhani, A., Makris, A., et al. (2016). Radiogenomics Monitoring in Breast Cancer Identifies Metabolism and Immune Checkpoints as Early Actionable Mechanisms of Resistance to Anti-angiogenic Treatment. EBioMedicine *10*, 109-116.

Mitsuhashi, A., Kiyokawa, T., Sato, Y., and Shozu, M. (2014). Effects of metformin on endometrial cancer cell growth in vivo: a preoperative prospective trial. Cancer *120*, 2986-2995.

Mullen, A.R., Wheaton, W.W., Jin, E.S., Chen, P.H., Sullivan, L.B., Cheng, T., Yang, Y., Linehan, W.M., Chandel, N.S., and DeBerardinis, R.J. (2011). Reductive carboxylation supports growth in tumour cells with defective mitochondria. Nature *481*, 385-388.

Niraula, S., Dowling, R.J., Ennis, M., Chang, M.C., Done, S.J., Hood, N., Escallon, J., Leong, W.L., McCready, D.R., Reedijk, M., et al. (2012). Metformin in early breast cancer: a prospective window of opportunity neoadjuvant study. Breast Cancer Res Treat *135*, 821-830.

Robey, R.B., and Hay, N. (2009). Is Akt the "Warburg kinase"?-Akt-energy metabolism interactions and oncogenesis. Semin Cancer Biol *19*, 25-31.

Robinson, M.D., McCarthy, D.J., and Smyth, G.K. (2010). edgeR: a Bioconductor package for differential expression analysis of digital gene expression data. Bioinformatics *26*, 139-140.

Schooneman, M.G., Vaz, F.M., Houten, S.M., and Soeters, M.R. (2013). Acylcarnitines: reflecting or inflicting insulin resistance? Diabetes *62*, 1-8.

Schuler, K.M., Rambally, B.S., DiFurio, M.J., Sampey, B.P., Gehrig, P.A., Makowski, L., and Bae-Jump, V.L. (2015). Antiproliferative and metabolic effects of metformin in a preoperative window clinical trial for endometrial cancer. Cancer Med *4*, 161-173.

Sonnenblick, A., Agbor-Tarh, D., Bradbury, I., Di Cosimo, S., Azim, H.A., Jr., Fumagalli, D., Sarp, S., Wolff, A.C., Andersson, M., Kroep, J., et al. (2017). Impact of Diabetes, Insulin, and Metformin Use on the Outcome of Patients With Human Epidermal Growth Factor Receptor 2-Positive Primary Breast Cancer: Analysis From the ALTTO Phase III Randomized Trial. J Clin Oncol *35*, 1421-1429.

Sullivan, L.B., Gui, D.Y., Hosios, A.M., Bush, L.N., Freinkman, E., and Vander Heiden, M.G. (2015). Supporting Aspartate Biosynthesis Is an Essential Function of Respiration in Proliferating Cells. Cell *162*, 552-563.

Wheaton, W.W., Weinberg, S.E., Hamanaka, R.B., Soberanes, S., Sullivan, L.B., Anso, E., Glasauer, A., Dufour, E., Mutlu, G.M., Budigner, G.S., et al. (2014). Metformin inhibits mitochondrial complex I of cancer cells to reduce tumorigenesis. Elife *3*, e02242.

Zhang, L., Han, J., Jackson, A.L., Clark, L.N., Kilgore, J., Guo, H., Livingston, N., Batchelor, K., Yin, Y., Gilliam, T.P., et al. (2016). NT1014, a novel biguanide, inhibits ovarian cancer growth in vitro and in vivo. J Hematol Oncol *9*, 91.

Main figure titles and legends:

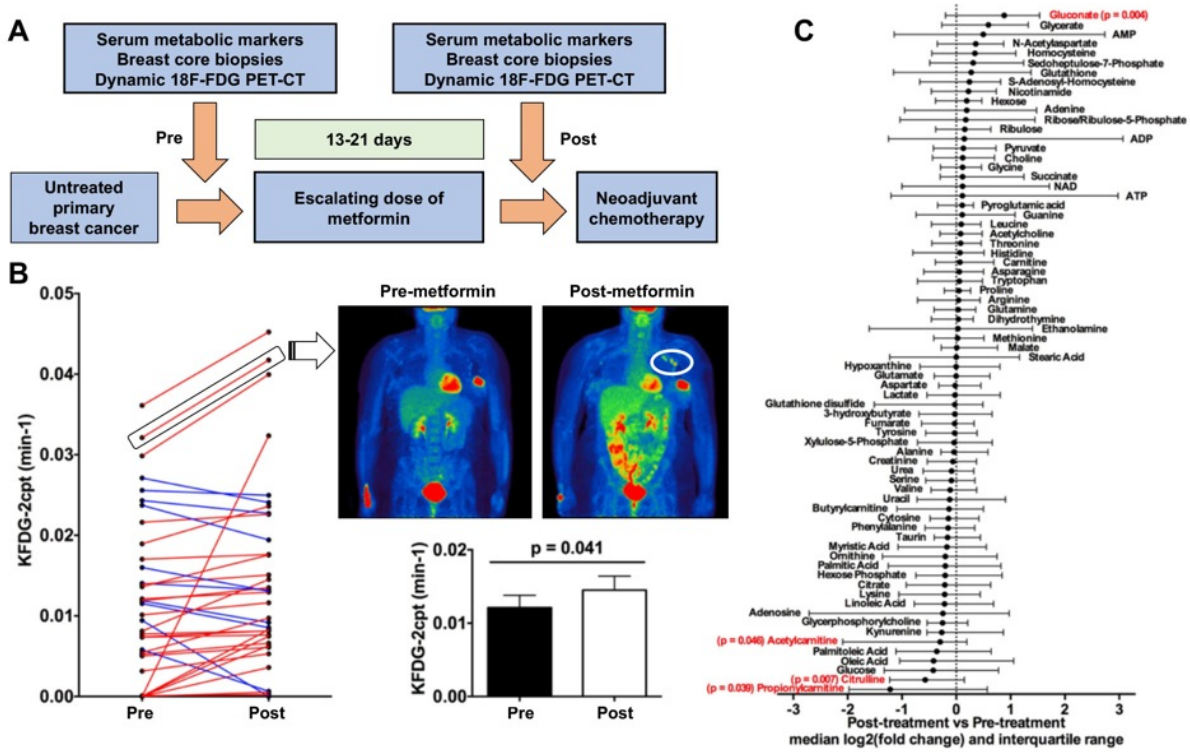

Fig. 1. Trial design and imaging analysis

(**A**): Study design. Shortly after diagnosis patients with untreated primary breast cancer received 13–21 days of slow release metformin at escalating dose-levels (500mg for days 1–3, 1000mg for days 4–6 and 1500mg thereafter) with core biopsies taken pre- and post-metformin before proceeding to neoadjuvant chemotherapy. (**B**): Change in the FDG flux constant $K_{FDG\text{-}2cpt}$ of the primary tumour in individual patients (left panel) and overall (lower right panel) pre- and post-metformin (n=36, paired t-test; data shown are mean ± SEM). Upper right panel: static PET-CT images in coronal plane pre- and post-metformin are from an individual with an increase in $K_{FDG\text{-}2cpt}$ following metformin; note increased uptake in axillary lymph nodes (circled). (**C**): Median fold change and interquartile range for metabolites pre- and post- metformin. Metabolites with statistically significant absolute change on Wilcoxon signed rank test are shown in red with p values (n=29). See also Figure S1 and Tables S1, S2 and S3.

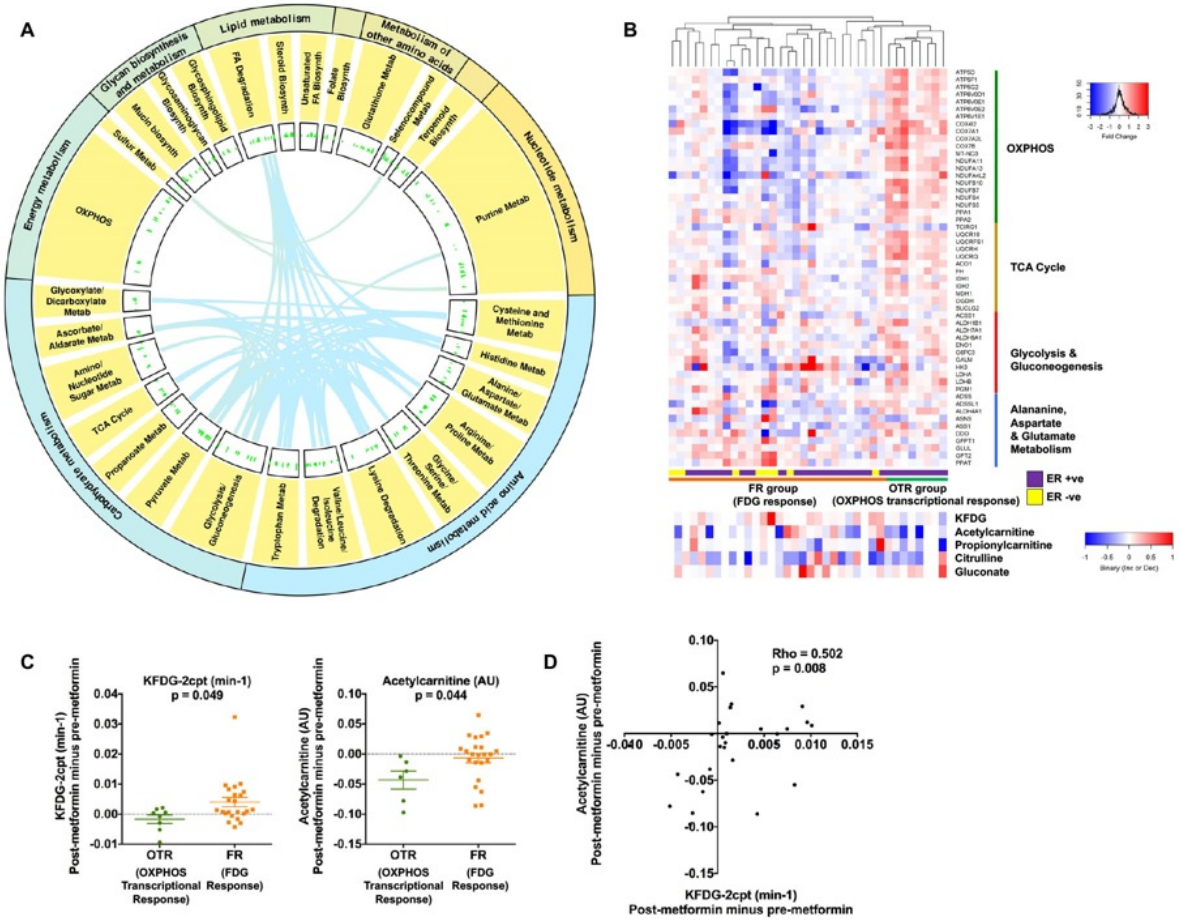

Fig. 2. Metformin alters levels of mitochondrial metabolites and increases OXPHOS relevant gene transcription in a subset of patients

(**A**): Circos plot to show all significantly upregulated metabolic pathways in the KEGG database. The width of the outer and inner circles show the mean relative abundances for the broadest hierarchy and secondary hierarchy. The bars in the innermost circle represent the mean relative abundances for genes encoding proteins within the individual pathways. The curved lines link genes that are shared among different pathways as indexed by KEGG (**B**): Heatmap of differentially expressed genes from the following KEGG pathways: oxidative phosphorylation (KEGG:00190); TCA cycle (KEGG:00020); glycolysis and gluconeogenesis (KEGG:00010); alanine, aspartate and glutamate metabolism (KEGG:00250). Each row represents a gene and each column represents a single patient (n=36). Colours reflect the fold change for each gene post-metformin: Red = up-regulation, Blue = down-regulation.

Samples were visually clustered using hierarchical clustering. OXPHOS transcriptional response group (OTR) and FDG response group (FR) shown. Shown below is heatmap of change in significantly altered metabolites and $K_{FDG\text{-}2cpt}$ (all post - pre) for same individual patients. (**C**): Scatter plot to show for the OXPHOS transcriptional response group (OTR) and FDG response group (FR) change in $K_{FDG\text{-}2cpt}$ and acetylcarnitine levels for the breast primary tumour (both post minus pre). Data shown are mean ± SEM, unpaired t-test. (**D**): Correlation between change in $K_{FDG\text{-}2cpt}$ and acetylcarnitine (both post minus pre). Spearman's rank correlation coefficient and significance, are shown. See also Figure S2 and Table S4.

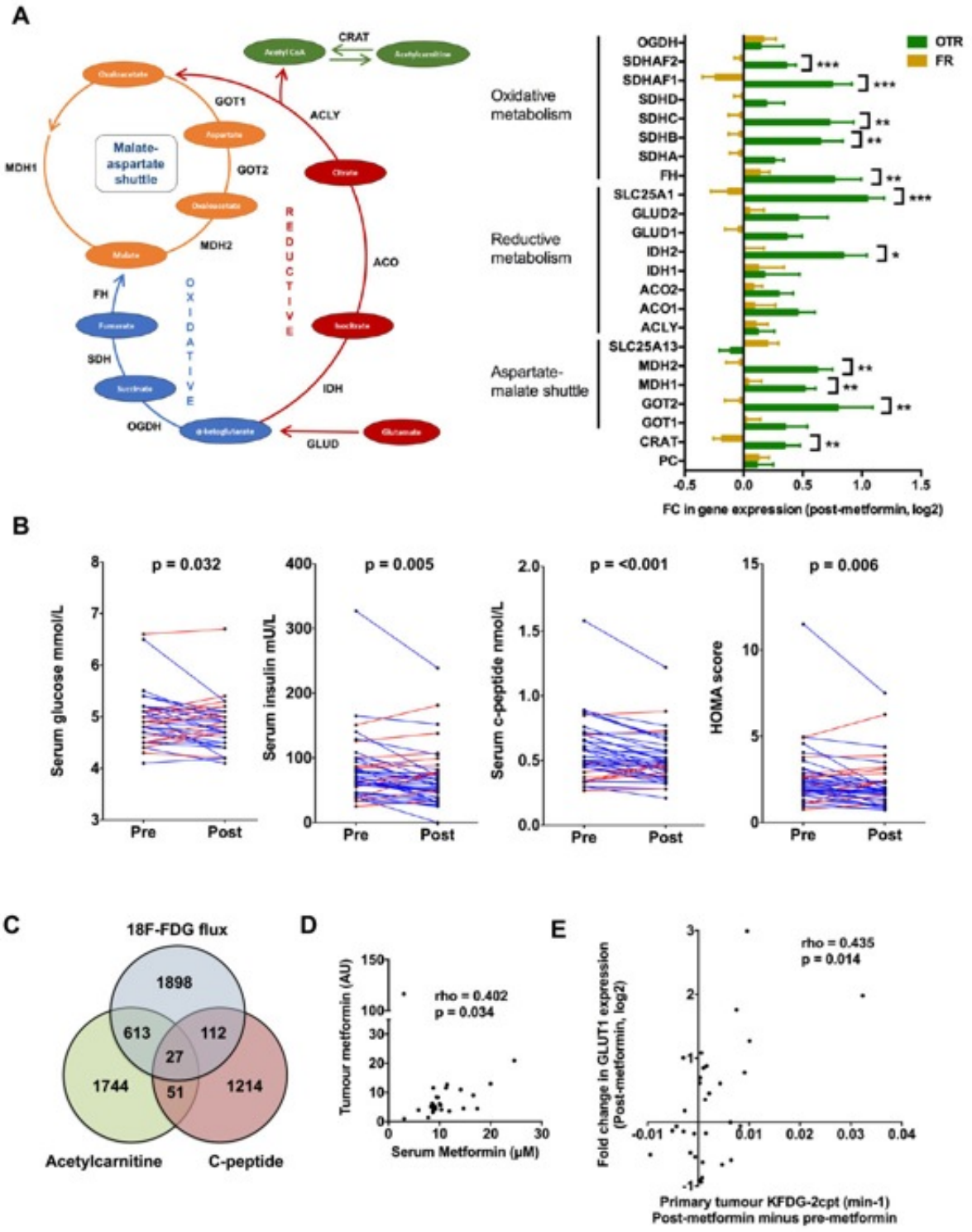

Fig. 3. Effect of metformin on systemic metabolism

(**A**): Change in expression of genes involved in regulation of aspartate/malate shuttle and oxidative and reductive metabolism, unpaired t-test (n=36). Data shown are mean ± SEM *p < 0.05; **p < 0.01; ***p < 0.001. (**B**): Pre- and post-metformin serum glucose, insulin, IGF-1

levels and HOMA score for individual patients. Significant decrease for each host metabolic marker, p-value shown (paired t-test, n=40). (**C**): Venn diagram to show overlap of all genes whose change in expression correlated with either change in systemic levels of circulating c-peptide or tumour $K_{FDG\text{-}2cpt}$ or tumour acetylcarnitine. (**D**): Correlation between peak serum metformin levels (2 hours post dose) and tumour metformin levels (**E**): Correlation between change in $K_{FDG\text{-}2cpt}$ (post-pre) and GLUT1 expression (log2FC) for the breast primary tumour. Spearman's rank correlation coefficient and significance, are shown for (D) and (E). See also Figure S3 and Tables S5 and S6.

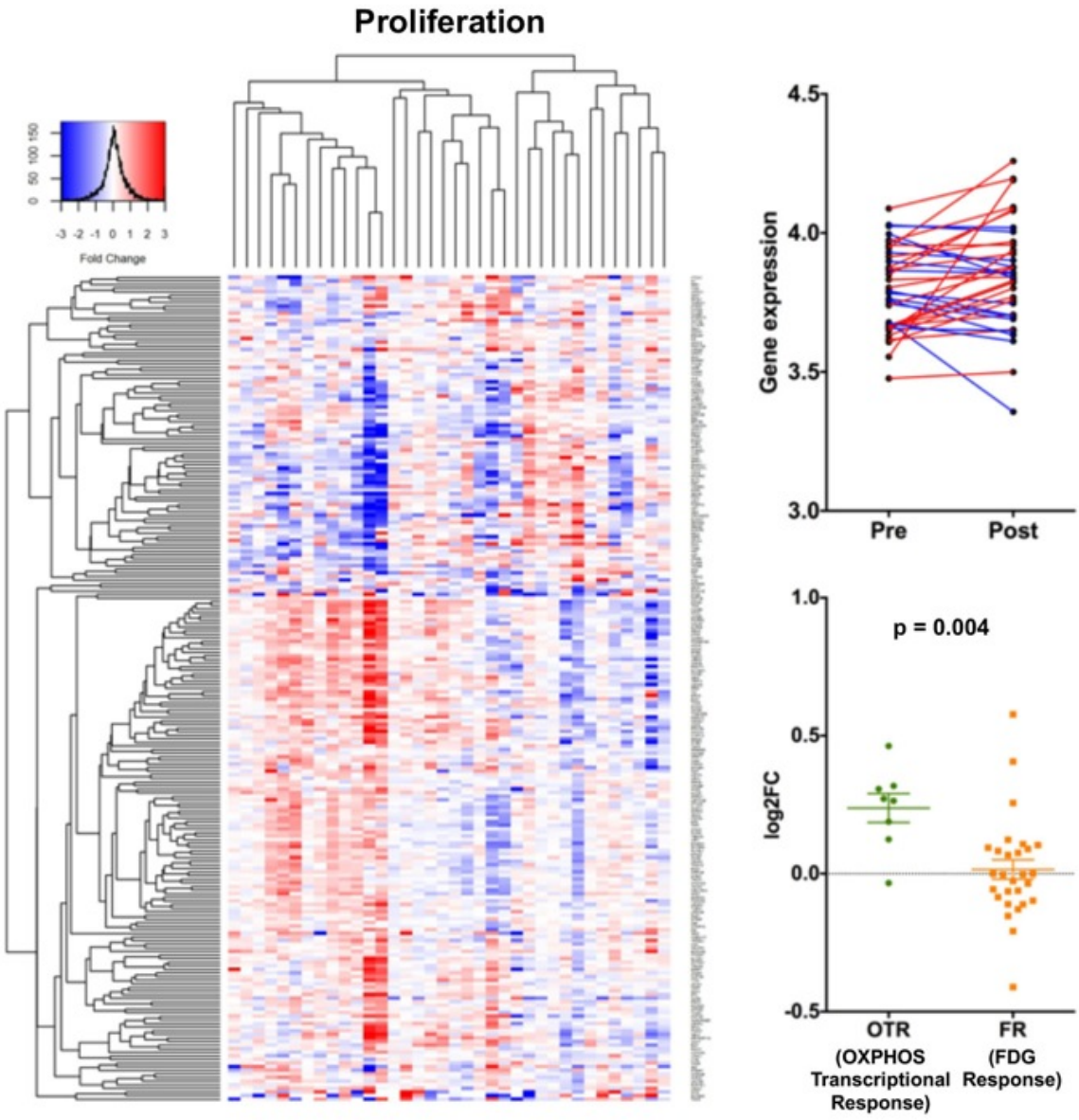

Fig. 4. Effect of metformin on proliferation

Left panel, heatmap of genes from the proliferation signature. Each row represents a gene and each column represents a single patient. Colours reflect the fold change for each gene post-metformin: Red = up-regulation, Blue = down-regulation. Samples were visually clustered using hierarchical clustering. Right upper panel, pre- and post-metformin expression of signatures for individual patients (n=36); Right lower panel, scatter plot to show change in expression of signatures for the OXPHOS transcriptional response group (OTR) and FDG response group (FR). Data shown are mean ± SEM, unpaired t-test (n=36).

STAR Methods:

CONTACT FOR RESOURCE SHARING

Further information and requests for resources should be directed to and will be fulfilled by the Lead Contact, Simon Lord (simon.lord@oncology.ox.ac.uk).

METHOD DETAILS

Clinical study design and patient selection

Patients were recruited from the medical oncology breast cancer clinic over a period of 30 months between May 2011 and November 2013 in three UK centres, Oxford, Luton and Dundee. Informed consent was obtained from all patients. The study was prospectively approved by the NHS Oxfordshire Research Ethics Committee A and registered with the ClinicalTrials.gov identifier: NCT01266486. All patients at the point of recruitment had been referred with a view to neoadjuvant chemotherapy, had histologically confirmed breast cancer and gave informed consent. In all cases the primary breast cancer was in situ and no patients had received any prior treatment for breast cancer. See **Table S1** for a list of key eligibility criteria. In total 41 patients were recruited and had evaluable data. See **Table S2** for numbers of patients with sufficient data for paired analysis for each assay. All patients were female and the median age at study entry was 49 years (range 27 – 67 years). Median body mass index at study entry was 28.1 (range 19.6 – 45.3).

Metformin was given in the Glucophage XR™ formulation in an escalating dose once daily for a minimum of 13 days and a maximum of 21 days (500mg for days 1–3, 1000mg for days 4–6 and 1500mg thereafter). The day prior to commencing metformin a core biopsy was taken under ultrasound guidance from the periphery of the primary tumour. Within 1 minute of this procedure the biopsy material was snap frozen in liquid nitrogen prior to

storage at -80 ^{o}C. Prior to metabolomics analysis biopsy samples were divided and one portion used for broad metabolomics analysis and the other to generate a lipid profile.

PET-CT protocol

The radiotracer, 2-deoxy-2-(18F)fluoro-D-glucose (^{18}[F]-FDG), was used for all examinations. Prior to scanning, patients were fasted overnight for at least 8 hours but could drink water. Patients' blood glucose was checked just prior to the scan with a portable blood glucose monitor to ensure it was <7mmol/L. All scans took place on either a 3D mode time of flight GE Discovery 690 64-slice PET-CT system (GE Healthcare, Milwaukee) or Siemens Biograph mCT-128 (Siemens Healthcare, Germany).

A dynamic acquisition of the breast tumour (and any lymph nodes within the PET field of view) was initiated with the patient imaged supine. Patients were injected with ^{18}[F]-FDG (3 MBq/kg, up to a maximum of 400 MBq) 30 seconds into PET imaging, which continued for 45 minutes. The 45 minutes of data were then reconstructed as a sequence of images describing average activity concentrations during a series of time frames (1x30s, 12x5s, 6x10s, 5x30s, 10x60s, 6x300s).

50 minutes after injection, a static PET scan was performed from skull base to mid-thigh, acquiring data for four minutes at each bed position. Thus the primary breast cancer was scanned at approximately 60 minutes post injection, in addition to the dynamic PET scanning from 0-45 minutes. Prior to each PET acquisition a CT scan was performed for localization and PET attenuation correction, using a pitch of 0.984, 120 kV, automA with a noise index of 25.

The PET images were reconstructed on a matrix of 5.5×5.5×3.3 mm^3 voxels using filtered back projection for the dynamic sequence, and iterative reconstruction for the static scan. See supplementary methods for further details of static and kinetic analysis of imaging.

Static PET-CT analysis

Tumour volumes were delineated on the 60-minute static FDG-PET scans by a nuclear medicine radiologist working on a Hermes workstation and using Hybrid viewer software (Hermes Medical Solutions AB, Stockholm, Sweden). Maximum and mean standardized uptake values (SUV) within each tumour volume were normalized by lean body mass (LBM) and reported as $SUL_{mean}=SUV_{mean}*LBM/BW$ and $SUL_{max}=SUV_{max}*LBM/BW$ respectively, where

$$\mathrm{LBM}_{\mathrm{Hume}} = \begin{cases} 0.32810 \times \mathrm{BW} + 0.33929 \times \mathrm{H} \times 29.5336\,(\mathrm{Males}) \\ 0.29569 \times \mathrm{BW} + 0.41813 \times \mathrm{H} \times 43.2933\,(\mathrm{Females}) \end{cases}$$

and BW and H are the body weight in kg and height in cm (Hume, 1966).

Dynamic PET-CT analysis

The tumour volume contoured on a static PET-CT image was transferred to the corresponding 0-45 minute dynamic FDG-PET scan by co-registering the two image sets. Time-activity curves (TACs) describing time-courses of mean tumour FDG activity concentration within the tumour were then calculated for the tumour regions of the dynamic scans. Time-courses of blood-borne tracer concentrations were similarly obtained from regions defined in the descending aorta (average 42 ± 4 slices with mean volume of 32 ± 11 cm^3), and used to describe tracer inflow into tumours ('input functions', IF).

Kinetic analysis of tumour FDG uptake was carried out for 36/40 patients, using irreversible 2- and 3-tissue compartment models (Bertoldo et al., 2001). Tumour TACS for the remaining four patients were not analysed as they showed pronounced discontinuities, likely due to movement during scanning. The compartment models characterize FDG transport and intracellular phosphorylation using a small number of parameters, and enable modelled tumour TACs to be calculated directly from IFs. The models were fitted by adjusting the

parameters to achieve the best weighted least-squares match between modelled and measured tumour TACs (Liu et al., 2014).

The 2-tissue compartment model (2cpt) provided better descriptions of tumour TAC data, judged by the Akaike and Bayesian information criteria (AIC and BIC) used alongside a runs-test. From each fit, estimated values and associated statistical uncertainties were obtained for the model parameters v_B, K_1, k_2 and k_3, which respectively describe the fractional tumour blood volume and rate-constants for FDG transport back and forth between the vasculature and tumour cells, and for intra-cellular phosphorylation. Uncertainties on these fitted parameters are quite large due to statistical noise in dynamic PET images. Flux constants K_{FDG}, numerically equal to $K_1k_2/(k_2+k_3)$, were also calculated. Conceptually K_{FDG} describes the rate of intra-cellular FDG phosphorylation when a steady-state unit concentration of FDG exists in the blood, and statistically it is estimated substantially more precisely than the individual model rate-constants. Figure S5 summarizes the analysis. Significances of differences in model parameters before and after metformin were assessed using paired t-test and Wilcoxon signed rank test. Only changes in K_{FDG} proved significant.

It was not useful to kinetically analyse FDG uptake time-courses in the axillary nodes, since the small nodal volumes led to a high degree of noise on the time-courses and fitted kinetics parameters including the flux constant. All patients included in the axillary node analysis who had lymph node avidity had evidence at pre-treatment biopsy or surgery of metastatic breast carcinoma involvement within the axillary nodes with the exception of 3 patients for whom no biopsy or surgical data was available.

Mass spectrometry analysis of clinical samples for metabolomic profile

Breast cancer tissue was pulverised via mechanical disruption (IKA Ultra-Turrax T-8 homogenizor) prior to hydrophilic extraction of intracellular metabolites from tissue using a methanol/acetonitrile/water (50/30/20) extraction solution (250 µL of extraction solution per 10mg homogenised tissue). Following thorough mixing, the samples were centrifuged for 10 minutes at 10,000G and the supernatant stored at -80^{o}C prior to mass spectrometry analysis.

For the LC separation, column A the sequant Zic-pHilic (150 mm × 2.1 mm i.d. 5 µm) with the guard column (20 mm × 2.1 mm i.d. 5 µm) from HiChrom, Reading, UK. Mobile phase A: 20 mM ammonium carbonate plus 0.1% ammonia hydroxide in water. Mobile phase B: acetonitrile. The flow rate was kept at 180 µL/minute and gradient as follow: 0–1 minutes 70% of B, 16 minutes 38% of B, 16.5 minutes 70% of B, 25 minutes 70% of B. The mass spectrometer (Thermo Q-Exactive Orbitrap) was operated in a polarity switching mode. Experimenters analysing samples from metabolomics experiments were blinded to the experimental interventions. Samples were randomised in order to avoid machine drifts.

Analysis of RNASeq data

Next generation sequencing of 'Poly (A) targeted' mRNA, including library preparation, was carried out by the Oxford Genomics Centre core facility at the Welcome Trust Centre for Human Genetics. The NEBNext mRNA Library Prep Master Mix Set (New England Biolabs) was used for preparation of the expression libraries and the Illumina HiSeq 2000 system used to carry out the sequencing.

Paired-read were aligned to human reference genome GRCh38, including transcriptomic information, by Bowtie 2.2.6 and Tophat v2.1. The fold change of normalized expression

level, FPKM (Fragments Per Kilobase of transcript per Million mapped reads), for each gene was then estimated from those aligned reads using Cuffdiff 2.2.1. Non-parametric rank product (R package and version) was used to discover the genes with consistent statistically significant fold change (probability of false positive < 0.05) between pre- and post-metformin treatment, among all patients were selected. This approach was preferred with respect to EdgeR (Anders and Huber, 2010) and Deseq (McCarthy et al., 2012; Robinson et al., 2010) as in datasets with high variability and paired samples (pre and post- treatment) non parametric methods tend to work better in our previous studies (Mehta et al., 2016); however analysis with EdgeR (version 3.16.5) and Deseq (version 1.26.0) was also done and did not change the main conclusions.

Measurement of circulating markers

Patient serum samples were collected after fasting overnight just prior to the breast core biopsy (and for the post-metformin sample 2 hours post-dose). Fasting glucose, insulin, c-peptide, c-reactive protein, leptin and adiponectin were measured using NHS biochemistry services to standardised and validated protocols. The homeostasis model assessment (HOMA) was calculated using the following equation: (glucose mmol/L * insulin mU/L)/22.5.

IL-6 and TNF-alpha were measured in duplicate by High Sensitivity enzyme linked immunosorbent assay (ELISA) (Invitrogen). These assays utilise two amplification steps, allowing for the detection of low levels of cytokines present in serum and plasma samples.

Immunohistochemistry

Staining for p-AMPK (1 in 200, thr172 residue, Cell Signaling Technologies #2535) and pAKT (1 in 100, ser473 residue, Cell Signaling Technologies #4060), was performed on a Leica Bond-max autostainer in the GCP laboratory, Department of Pharmacology, University of Oxford. For pAMPK, cell pellet controls were generated using MCF7 cells treated with either 20 μM Compound C (negative control) or 250 μM AICAR (positive control) for 24 hours prior to harvesting. For pAKT, cell pellet controls were generated using serum starved MCF7 cells either untreated (negative control) or treated with IGF-1 (positive control) for 30 minutes prior to harvesting and the generation of a formalin fixed, paraffin embedded cell pellet block.

Quantitative scoring of the staining of complete tumour sections was evaluated by two accredited pathologists using high power fields the intensity of the immunostaining was classified into 4 categories: 0, no immunostaining present; 1, weak staining; 2, moderate staining; and 3, strong staining and the percentage of positive cells at each intensity was then classified into 4 groups; 1 (0-10% positive cells), 2 (11% to 50% positive cells), 3 (51% to 80% positive cells) or 4 (81 to 100% positive cells). The H-score of immunoreactivity was obtained by multiplying the intensity and percentage scores.

QUANTIFICATION AND STATISTICAL ANALYSIS

Processing for dynamic PET-CT and gene expression profiling are reported above. Absolute difference in metabolites was analysed using paired non-parametric method (Wilcoxon Signed Rank Sum). All other differences in measurements pre- and post-metformin were compared using paired t-tests. Correlation analyses between gene expression scores, metabolites, metformin levels, circulating metabolic markers and K_{FDG} were performed using non-parametric methods (Spearman's rank correlation coefficient). Differences in

measurements between the OTR and FR groups were examined using an unpaired two-tailed t-test. Statistical tests for each analysis are defined in figure legends. In all cases a p-value <0.05 was considered significant. Analysis of RNASeq and Metabolomic data was carried out using non-parametric approaches and hence the data was not required to follow an underlying distribution. Kinetic model fits to the tumour TACs extracted from dynamic PET scans were runs-tested as a non-parametric check on fit quality. Significances of pre/post metformin differences in PET tracer kinetics parameters and normalised static uptake values were assessed using a parametric t-test and a non-parametric Wilcoxon signed rank test, the assumption of normally-distributed data underlying the t-test being rejectable with $p<.05$ for all variables except K1 according to the Shapiro-Wilk test. Statistical packages, GraphPad PRISM v6.0, R v3.3.1 and Matlab were used for analyses.

Sample size estimation:

Based on our and others' previous analyses of microarray data, a minimum of 20 cases with paired measurements at two time points were estimated to be sufficient to observe expression changes of at least 1.7-fold in genes showing a coefficient of variation at each time point up to 50% with a significance level after multiple test correction of $p=0.05$ (taking into account filtering of not expressed transcripts) and an 80% power. This estimate assumed uniformity of drug response. However, double the number was desirable for higher significance and considering correlation with baseline expression and response.

DATA AND SOFTWARE AVAILABILITY

The RNASeq gene expression data reported in this paper have been reported in Mendeley data with address doi: 10.17632/cytrpb62f2.1

ADDITIONAL RESOURCES

ClinicalTrials.gov Identifier: NCT01266486

KEY RESOURCES TABLE

REAGENT or RESOURCE	SOURCE	IDENTIFIER
Antibodies		
pAMPK thr172 residue	Cell Signaling Technologies	AB_331250
pAKT ser473 residue	Cell Signaling Technologies	AB_2315049
Critical Commercial Assays		
IL-6	Invitrogen	BMS213HS
TNF-alpha	Invitrogen	BMS223HS
NEBNext mRNA Library Prep Master Mix Set	New England Biolabs	E6110
Deposited Data		
Analysed RNASeq data	This paper	doi:10.17632/cytrpb62f2.1
Software and Algorithms		
RNASeq analysis	R-project	v3.3.1
Imaging analysis	Matlab	
Other statistical analyses	GraphPad PRISM	v6.0
Other		
Metformin	Bristol-Myers Squibb	Glucophage XR™
ClinicalTrials.gov Identifier	N/A	NCT01266486

Supplemental information

Integrated pharmacodynamic analysis identifies two metabolic adaption pathways to metformin in breast cancer

Authors:

Simon. R. Lord, Wei-Chen. Cheng, Dan. Liu, Edoardo. Gaude, Syed. Haider, Tom. Metcalf, Neel. Patel, Eugene. J. Teoh, Fergus. Gleeson, Kevin. Bradley, Simon. Wigfield, Christos. Zois, Daniel. R. McGowan, Mei-Lin. Ah-See, Alastair. M. Thompson, Anand. Sharma, Luc. Bidaut, Michael. Pollak, Pankaj. G. Roy, Fredrik. Karpe, Tim. James, Ruth. English, Rosie. F. Adams, Leticia Campo, Lisa. Ayers, Cameron Snell, Ioannis Roxanis, Christian. Frezza, John. D. Fenwick, Francesca. M. Buffa, Adrian. L. Harris

Inventory of Supplemental Information

SUPPLEMENTAL FIGURES:

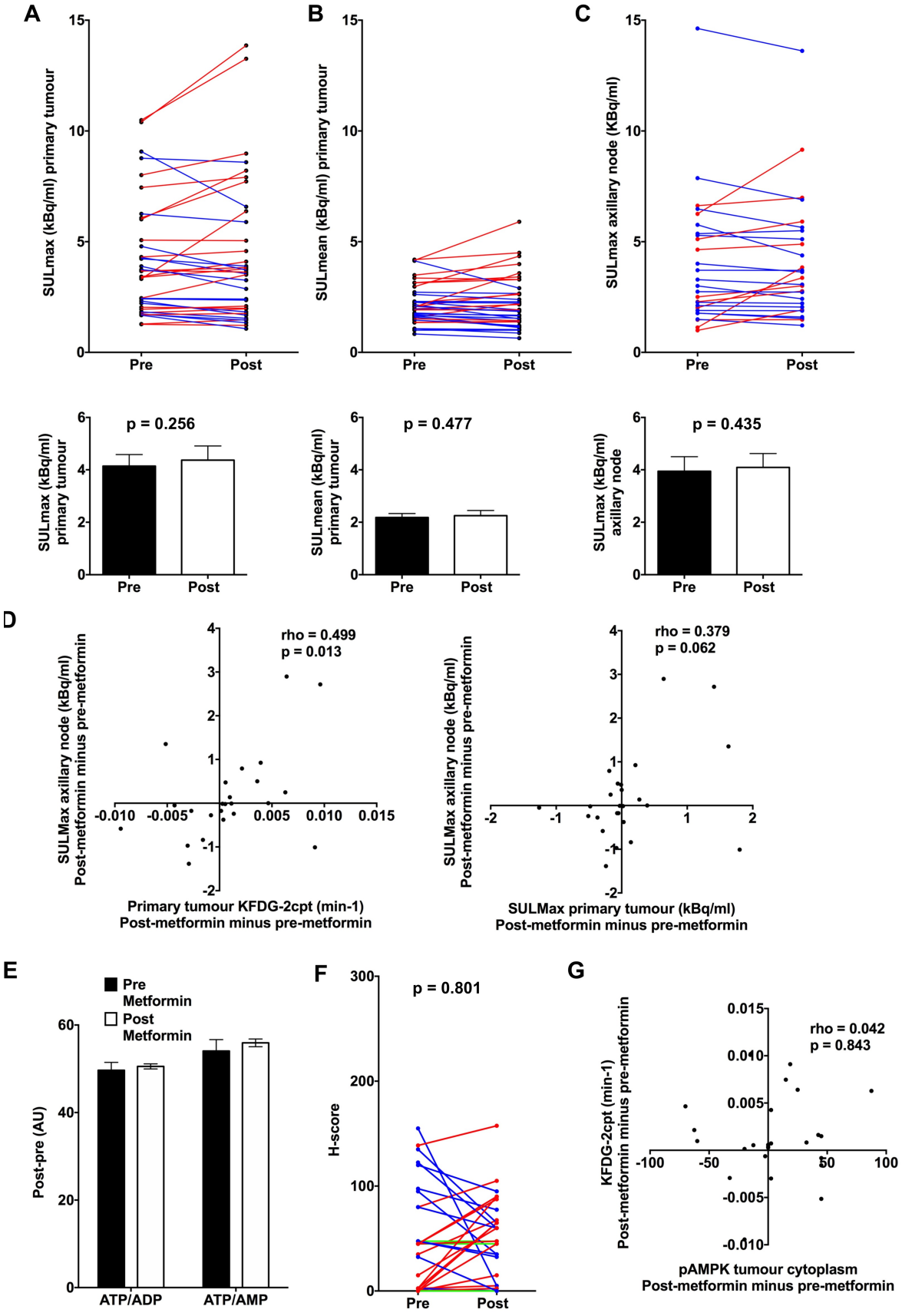
A
B
C
SULmax (kBq/ml) primary tumour
SULmean (kBq/ml) primary tumour
SULmax axillary node (KBq/ml)
Pre
Post
p = 0.256
p = 0.477
p = 0.435
SULmax (kBq/ml) primary tumour
SULmean (kBq/ml) primary tumour
SULmax (kBq/ml) axillary node
D
rho = 0.499
p = 0.013
rho = 0.379
p = 0.062
SULMax axillary node (kBq/ml) Post-metformin minus pre-metformin
Primary tumour KFDG-2cpt (min-1) Post-metformin minus pre-metformin
SULMax primary tumour (kBq/ml) Post-metformin minus pre-metformin
E
Pre Metformin
Post Metformin
Post-pre (AU)
ATP/ADP
ATP/AMP
F
p = 0.801
H-score
G
rho = 0.042
p = 0.843
KFDG-2cpt (min-1) Post-metformin minus pre-metformin
pAMPK tumour cytoplasm Post-metformin minus pre-metformin

Fig. S1. Effect of metformin on standardised uptake value of primary breast tumour. Related to Figure 1.

Change in the (**A**) maximum and (**B**) mean standardised uptake value normalised to lean body mass of the primary tumour in individual patients (upper panel) and overall (lower panel; data shown are mean ± SEM) pre- and post-metformin (n=36). (**C**): Change in maximum standardised uptake value normalised to lean body mass of axillary nodes in individual patients pre- and post-metformin (n=27). (**D**): Correlation between change in $K_{FDG\text{-}2cpt}$ (post-metformin minus pre-metformin) and SUL_{Max} for the breast primary tumour, respectively, and change in SUL_{Max} for FDG avid axillary lymph nodes. Spearman's rank correlation coefficient and significance, are shown. (**E**): ATP/AMP and ATP/ADP ratios pre- and post-metformin (n=29); data shown are mean ± SEM. (**F**): Change in pAMPK of primary tumour measured by immunohistochemistry in individual patients pre- and post-metformin (n=32; red = increase, blue = decrease and green = no change). (**G**): Correlation between change in $K_{FDG\text{-}2cpt}$ and pAMPK for the breast primary tumour (both post-metformin minus pre-metformin). Spearman's rank correlation coefficient and significance, are shown.

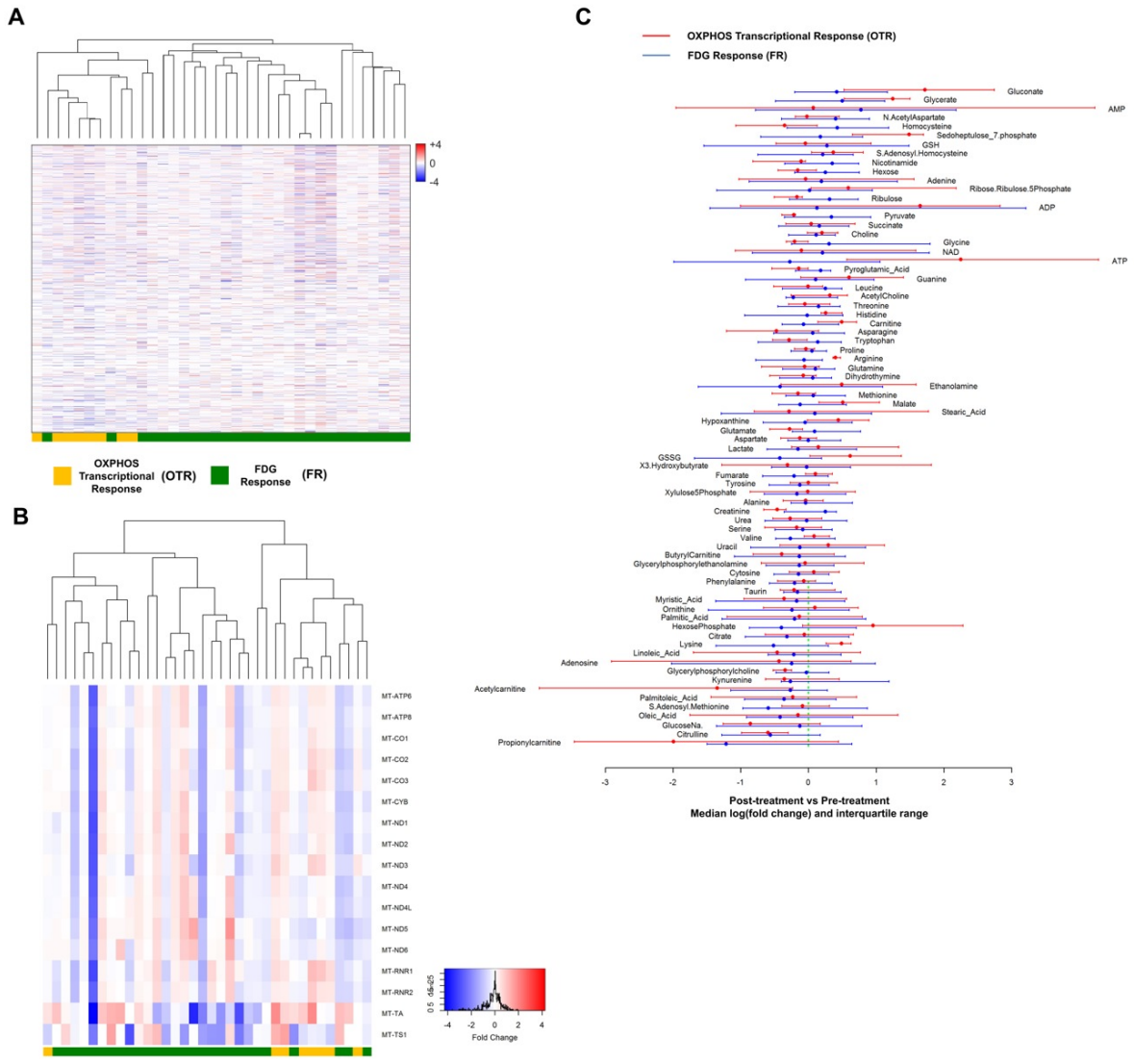

Fig. S2. Heatmaps of all expressed nuclear and mitochondrial encoded genes following metformin. Related to Figure 2.

Heatmaps of all expressed nuclear (**A**) and mitochondrial (**B**) encoded genes following metformin. Each row represents a gene and each column represents a single patient. Colours reflect the fold change for each gene post-metformin: Red = up-regulation, Blue = down-regulation. Samples were visually clustered using hierarchical clustering (n=36). Patients in OTR (orange) and FR (green) groups shown below. (**C**): Median log

FC and interquartile range for metabolites in OXPHOS transcriptional response (OTR) and FDG response groups.

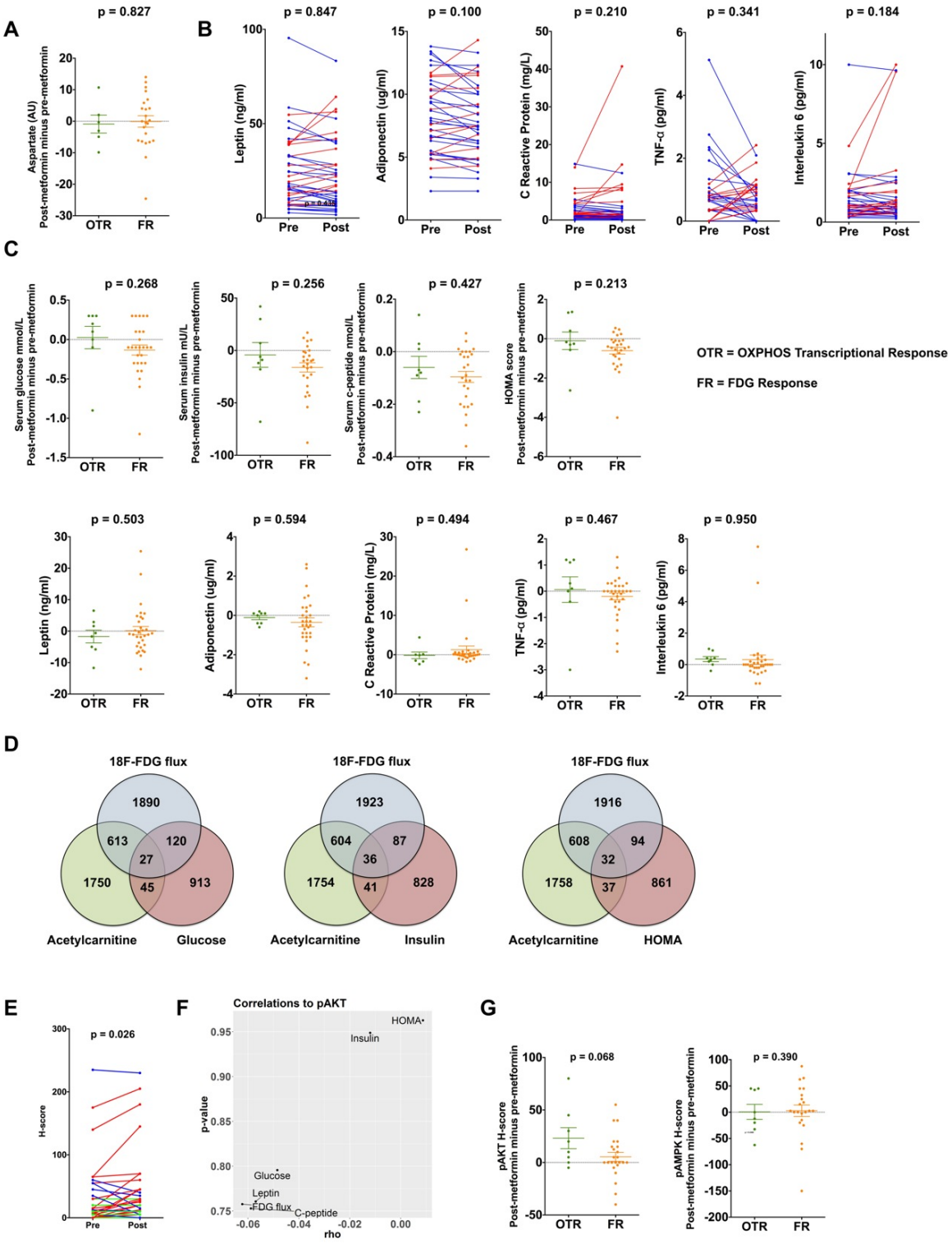

Fig. S3. Relationship between systemic effects of metformin and tumour metabolic response. Related to Figure 3.

(**A**): Scatter plot to show change in tumour aspartate levels for the OTR and FR groups (post-metformin minus pre-metformin). Data shown are mean ± SEM and p-value on unpaired t-test (n=29). (**B**): Pre- and post-metformin levels of serum leptin, adiponectin, C-reactive protein, tumour necrosis factor-alpha and interleukin-6 for individual patients (n=40). (**C**): Scatter plots to show for the OTR and FR groups change in the systemic metabolic markers, serum glucose, serum insulin, serum c-peptide, HOMA, leptin and adiponectin, and the systemic inflammatory markers, C-reactive protein, tumour necrosis factor-alpha and interleukin-6 (all post-metformin minus pre-metformin). Data shown are mean ± SEM and p-value on unpaired t-test (n=36). (**D**): Venn diagram to show overlap of all genes whose change in expression correlated with change in tumour $K_{FDG\text{-}2cpt}$ and tumour acetylcarnitine and either HOMA, or systemic levels of circulating glucose or insulin. (**E**): Change in pAKT of primary tumour measured by immunohistochemistry in individual patients pre- and post-metformin (n=32; red = increase, blue = decrease and green = no change). (**F**): Relationship between change in tumour pAKT and circulating metabolic markers (all post-metformin minus pre-metformin). Spearman's rank correlation coefficient and significance, are shown (n=27). (**G**): Scatter plots to show change in pAKT and pAMPK of primary tumour for the OTR and FR groups (both post-metformin minus pre-metformin). Data shown are mean ± SEM and p-value on unpaired t-test (n=32). (**H**): Examples of pAKT immunohistochemical staining for individual patients, upper panel: increase after metformin; lower panel: no change after metformin.

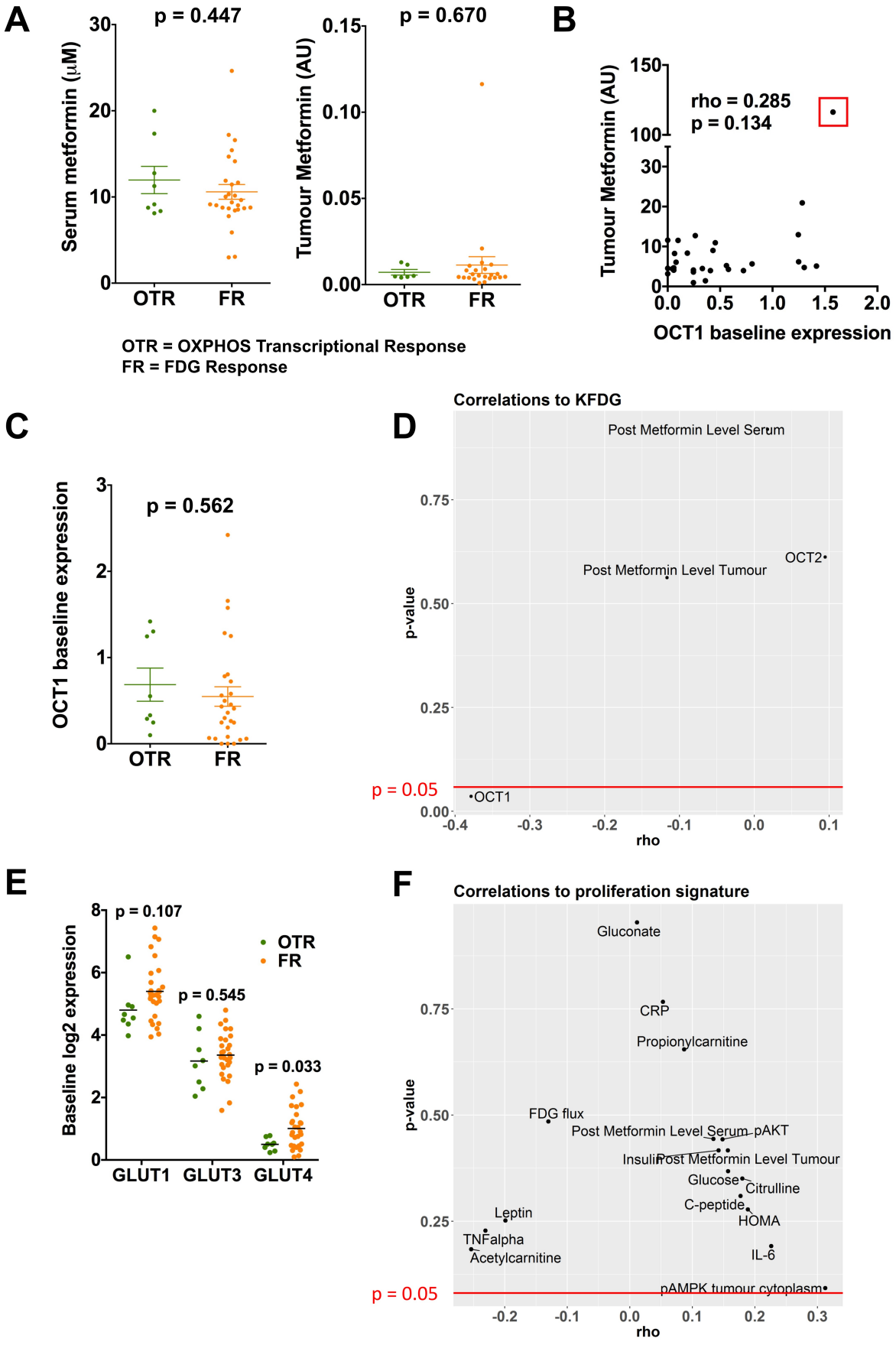

Fig. S4. Relationship between systemic effects of metformin and tumour

metabolic/proliferation response. Related to Figure 3.

(**A**): Scatter plots to show serum (n=35) and tumour metformin levels (n=29) for the OTR and FR groups. Data shown are mean ± SEM, on unpaired t-test. (**B**): Correlation between tumour metformin levels and OCT1 baseline expression, patient with highest OCT1 expression and metformin level indicated Venn diagram to show overlap of all genes whose change in expression correlated with change in tumour $K_{FDG\text{-}2cpt}$ and tumour acetylcarnitine and either HOMA, or systemic levels of circulating glucose or insulin. (**C**): Scatter plot to show baseline OCT1 gene expression for the OTR and FR groups. Data shown are mean ± SEM, on unpaired t-test. (n=36) (**D**): Relationship between change in tumour $K_{FDG\text{-}2cpt}$ and OCT1, OCT2, tumour and serum metformin levels (all post-metformin minus pre-metformin). Spearman's rank correlation coefficient and significance, are shown. (**E**): Scatter plot to show for the OXPHOS transcriptional response group (OTR) and FDG response group (FR) change in GLUT1, GLUT3, and GLUT4 expression (log2FC) for the breast primary tumour (GLUT2 not expressed in most tumours). Data shown are mean ± SEM, unpaired t-test (n=36). (**F**): Relationship between change in proliferation gene signature (log2FC) with circulating or tumour immunohistochemical markers, metformin levels, K_{FDG}, or significantly altered tumour metabolites. Spearman's rank correlation coefficient and significance, are shown.

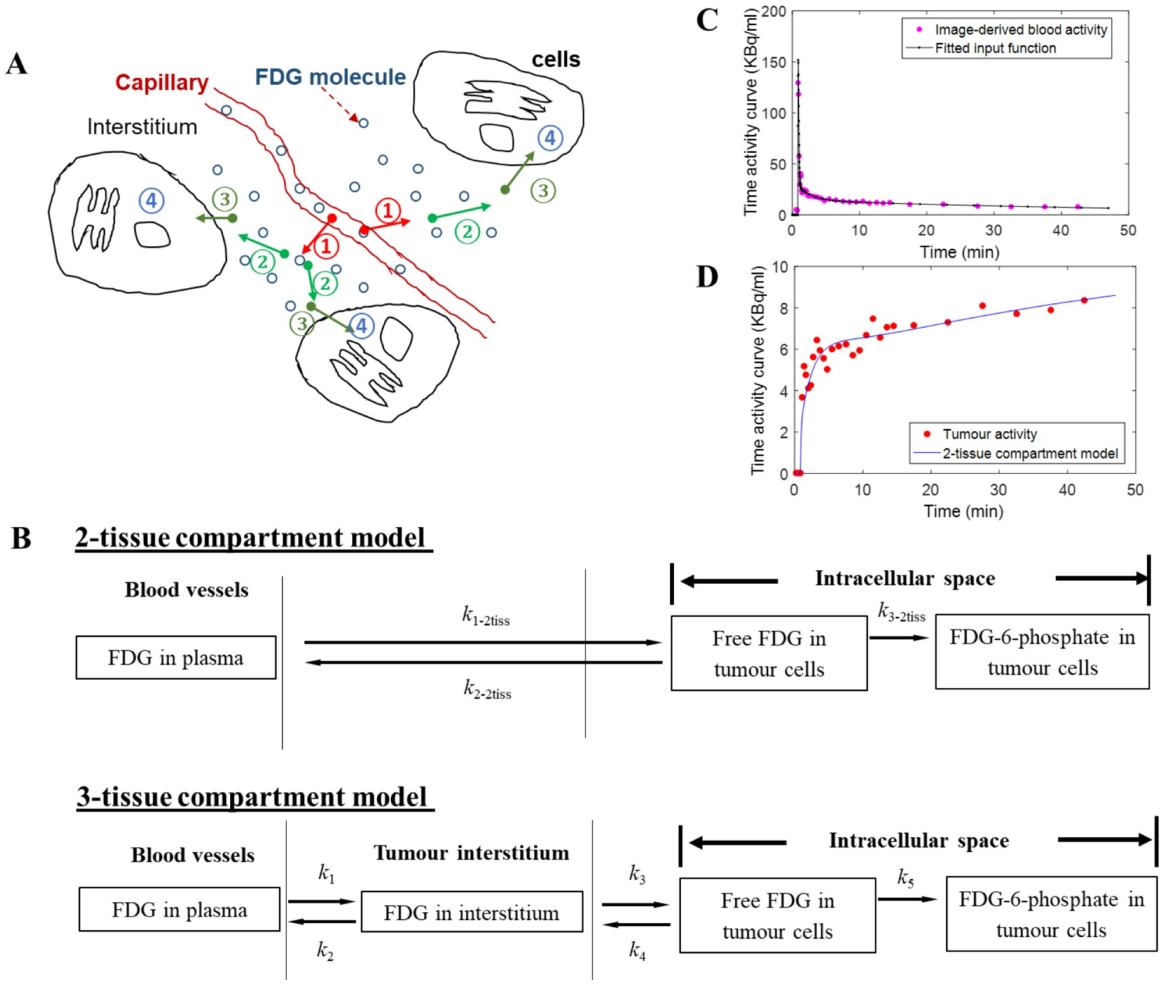

Fig. S5. Mechanism and modelling of 18F-FDG. Related to 'Dynamic PET-CT analysis' of STAR methods section.

(**A**) 18F-FDG tumour uptake occurs via: ① trans-capillary exchange; ② diffusion through the tumour interstitium; ③ trans-membrane transport to tumour intracellular spaces; and ④ intracellular phosphorylation of 18F-FDG. (**B**): two- and three-tissue compartment models describing 18F-FDG tumour uptake. (**C**): example of an image-derived blood input function, and (**D**): fit of the irreversible 2-tissue compartment model (continuous curve) to FDG uptake time-course data (dots) extracted from dynamic images for one patient.

SUPPLEMENTAL TABLES:

Inclusion criteria	Exclusion criteria
Women with a histology proven in situ primary breast cancer ≥2 cm in diameter	Radiotherapy, major surgery, significant traumatic injury, endocrine therapy, immunotherapy, chemotherapy or experimental therapy during four weeks prior to starting or during trial
Eastern Cooperative Oncology Group (ECOG) performance status 0−1	Pregnancy or breast feeding
Age ≥18 years	History of type 1 or type 2 diabetes
Fasting or random serum glucose less than 7.0 mmol/L	Treatment with metformin in the past year
No prior treatment for breast cancer and scheduled to commence neoadjuvant chemotherapy in ≤3 weeks time	Estimated glomerular filtration rate <45ml/min
Have given written informed consent and are capable of cooperating with protocol	Acute or chronic metabolic acidosis
Adequate bone marrow, renal and liver function	Known hypersensitivity to metformin

Table S1. List of key inclusion and exclusion criteria. Related to Figure 1.

			Number of patients
Recruitment and samples analysed	Total patient recruitment to study		41
	Number of paired PET-CT scans available for analysis		36
	Number of paired tumour samples with sufficient material for analysis	Metabolomics	29
		RNASeq	36
ER/HER2 status	ER positive		32
	ER negative		9
	HER2 positive		8
	HER2 negative		33
	Triple negative (ER negative and HER2 negative)		8
Tumour type	Ductal carcinoma		32
	Lobular carcinoma		7
	Mixed ductal and lobular carcinoma		2
	Grade 1		2
	Grade 2		24
	Grade 3		15
	Median tumour size (on magnetic resonance imaging)		49mm (range 30−147)
Patient characteristics	Median age at study entry		49 years (range 27−67)
	Median body mass index		28.1 (range 19.6−45.3

Table S2. Tumour and patient characteristics (for the 29 paired samples included in the general metabolomics analysis). Related to Figure 1.

Dynamic Imaging Variable	**p-value**		
	Paired t-test	**Wilcoxon**	**Mann-Whitney**
K1	0.145	0.162	0.341
k2	0.055	0.128	0.521
k3	0.343	0.053	0.392
Kflux (KFDG-2cpt(min-1)	0.041	0.027	0.510
SUVmean	0.918	0.271	0.356
TBRmean	0.255	0.540	0.540
MRglu	0.141	0.285	0.285

Table S3. P-values for all dynamic imaging variables using 3 different statistical tests, 2-tailed paired t-test; 2-sided Wilcoxon signed rank test; Mann-Whitney U-test. Related to Figure 1.

Pathway	KEGG ID	p-value*
Peroxisome	04146	<0.001
Arginine & proline metabolism	00330	<0.001
Valine, leucine & isoleucine degradation	00280	<0.001
Pyruvate metabolism	00620	0.001
Glutathione metabolism	00480	0.002
Citrate cycle	00020	0.004
Propanoate metabolism	00640	0.005
Fatty acid degradation	00071	0.005
Alanine & aspartate & glutamate metabolism	00250	0.005
Cysteine & methionine metabolism	00270	0.007
Lysine degradation	00310	0.009
Glycine, serine & threonine metabolism	00260	0.011
Huntingdon's disease	05016	0.016
Histidine metabolism	00340	0.023
PPAR signalling pathway	00320	0.030
Oxidative phosphorylation	00190	0.033
Ascorbate & aldarate metabolism	00053	0.033
Alzheimer's disease	05010	0.034
Glycolysis & gluconeogenesis	00010	0.040

Table S4. List of KEGG pathways linked to mitochondrial metabolism that were significantly upregulated following metformin treatment. * corrected Hypergeometric p-value. Related to Figure 2.

Circulating marker	Pre-metformin		Post-metformin		p-value*
	Mean	SEM	Mean	SEM	
Glucose (mmol/L)	4.94	0.08	4.82	0.45	0.032
Insulin (mU/L)	81.0	8.01	70.2	6.93	0.005
C-peptide (nmol/L)	0.59	0.04	0.50	0.03	<0.001
HOMA score	2.60	0.28	2.17	0.22	0.006
Leptin (ng/ml)	24.3	3.05	24.1	3.08	0.847
Adiponectin (ug/ml)	8.26	0.49	7.92	0.48	0.100
C-reactive protein (mg/L)	2.75	0.54	3.76	1.12	0.210
Tumour necrosis factor alpha (pg/ml)	0.74	0.16	0.60	0.10	0.341
Interleukin 6 (pg/ml)	1.50	0.26	1.82	0.40	0.184

Table S5. List of circulating markers tested. SEM, standard error of mean. * 2-tailed paired t-test. Related to Figure 3.

Gene	Full name	Brite hierarchy	
COX7B	cytochrome c oxidase subunit 7B	Energy metabolism	Oxidative phosphorylation
NDUFA4	NDUFA4, mitochondrial complex associated	Energy metabolism	Oxidative phosphorylation
NDUFS4	NADH:ubiquinone oxidoreductase subunit S4	Energy metabolism	Oxidative phosphorylation
AMY2B	amylase, alpha 2B (pancreatic)	Carbohydrate metabolism	Starch and sucrose metabolism
FBP1	fructose-bisphosphatase 1	Carbohydrate metabolism	Glycolysis / Gluconeogenesis
			Pentose phosphate pathway
			Fructose and mannose metabolism
GALK1	galactokinase 1	Carbohydrate metabolism	Galactose metabolism
			Amino sugar and nucleotide sugar metabolism
GYS1	glycogen synthase 1	Carbohydrate metabolism	Starch and sucrose metabolism
MGAM2	maltase-glucoamylase 2 (putative)	Carbohydrate metabolism	Galactose metabolism
			Starch and sucrose metabolism
PLCG1	phospholipase C gamma 1	Carbohydrate metabolism	Inositol phosphate metabolism
DNMT3B	DNA methyltransferase 3 beta	Amino acid metabolism	Cysteine and methionine metabolism
GCLC	glutamate-cysteine ligase catalytic subunit	Amino acid metabolism	Cysteine and methionine metabolism
			Glutathione metabolism
POLR2J2	RNA polymerase II subunit J2	Nucleotide metabolism	Purine metabolism
			Pyrimidine metabolism

POLR3GL	RNA polymerase III subunit G like	Nucleotide metabolism	Purine metabolism
			Pyrimidine metabolism
UBP1	beta-ureidopropionase 1	Nucleotide metabolism	Pyrimidine metabolism
		Metabolism of other amino acids	beta-Alanine metabolism
		Metabolism of cofactors and vitamins	Pantothenate and CoA biosynthesis
		Xenobiotics biodegradation and metabolism	Drug metabolism - other enzymes
HGSNAT	heparan-alpha-glucosaminide N-acetyltransferase	Glycan biosynthesis and metabolism	Glycosaminoglycan degradation
MAN2A2	mannosidase alpha class 2A member 2	Glycan biosynthesis and metabolism	N-Glycan biosynthesis
ST3GAL1	ST3 beta-galactoside alpha-2,3-sialyltransferase 1	Glycan biosynthesis and metabolism	Mucin type O-glycan biosynthesis
			Glycosaminoglycan biosynthesis - keratan sulfate
			Glycosphingolipid biosynthesis - globo and isoglobo series
			Glycosphingolipid biosynthesis - ganglio series
NADSYN1	NAD synthetase 1	Metabolism of cofactors and vitamins	Nicotinate and nicotinamide metabolism

Table S6. List of all KEGG annotated metabolism genes whose change in expression correlated with both change in tumour $K_{FDG\text{-}2cpt}$ and tumour acetylcarnitine levels. Related to Figure 3.